Microfluidic device incorporating closed loop feedback control for uniform and tunable production of micro-droplets

Erik Miller,[a] Mario Rotea[b] and Jonathan P. Rothstein*[a]

Received 3rd December 2009, Accepted 2nd February 2010
First published as an Advance Article on the web 25th February 2010
DOI: 10.1039/b925497h

Both micro- and nanofluidics are finding increasing use in the growing toolbox of nanotechnology; for the production of nanoparticles, and as micro-reactors for carefully controlled chemical reactions. These laboratories-on-a-chip hold vast potential for industrial application, however, only the most simple are truly starting to emerge as commercially viable, particularly in the area of droplet formation and emulsion creation. In order to automate droplet production with a desired size and dispersity, we have designed a microfluidic-based technology utilizing elementary microchannel geometries in combination with a closed loop feedback system to control the continuous- and dispersed-phase flow rates. Both the device geometry and control system have been optimized to allow for the production of a tunable emulsion. By utilizing discrete linear control theory, the device is able to produce the desired results with little to no prior knowledge of the fluid material properties to be used in either phase. We present our results from initial development using flow-focusing microfluidic geometry for droplet formation, computer-tethered syringe pumps to individually control the continuous and dispersed phase flow rates, a high-speed camera, and a controller and driver system for the optical measurements and pumps, respectively. We will show the efficacy of this technique for Newtonian and viscoelastic liquids, with and without the presence of surfactants. It can be envisioned that through careful control optimization, such a system can be developed to a point that will allow the production of "designer" emulsions with droplets eventually reaching the nanoscale.

1. Introduction

Microfluidics is defined as the science and technology of systems that process or manipulate very small amounts of fluids (microlitre and smaller) using devices comprised of channels with dimensions on the order of micrometres.[1] It is the small size scale that gives microfluidic devices some highly beneficial properties in a range of applications. Purely in terms of size and volume characteristics, minuscule amounts of fluid samples and reagents can be used to perform experiments at a low-cost, in a shorter time, and on a very small device footprint.[2] This has been widely exploited over the last 15 years for a variety of applications primarily in the fields of micro-analysis and micro-chemistry for separation and detection with high-resolution and sensitivity.[1] The physics of the fluid flow through microchannels within a microfluidic device is interesting and often counterintuitive.[3] The flow regimes are confined to low Reynolds numbers as a result of the disparately small length scales, thereby remaining laminar even for fluids with low viscosities and at high flow rates. This creates an inherently non-mixing environment and allows for the precise control and manipulation of multiple phases.

Stable droplets of one fluid in another, emulsions, are highly useful in a range of applications from personal care products, to foods, as well as drug delivery vehicles. Control over the size and distribution of such droplets is the critical element in such micro- and nano-emulsions.[4] Emulsions are traditionally formed using a "top-down" approach, wherein turbulence is used to break apart an immiscible mixture into small droplets. Conversely, a "bottom-up" approach is possible in microfluidic devices, where droplets are in fact formed within a continuous phase. Several methods have been explored and recently reviewed,[5] including colliding jets, cross-flowing or T-junctions, and co-flowing or flow-focusing. Experiments with high pressure injection of jets within a microfluidic device have been used to form concentrated nano-emulsions,[6] however, they require multiple further refining steps due to the lack of control in dispersity from jet collisions. The simple shearing cross-flow of a continuous phase past a T-junction geometry introducing a dispersed phase has been proven as a simple and effective method of creating stable and monodisperse droplets with a variety of systems.[7–9] In the co-flowing method, droplets are created by focusing a stream of fluid between a co-flowing immiscible fluid.[4,10] The formation of a central microthread and tip streaming has allowed this method to create smaller droplets with a controlled polydispersity.[11] Additionally, although the flow-focusing geometry is more complex, the nature of the flow has provided more control, allowing very interesting results including the creation of gas microbubbles in a continuous liquid phase[12] as well as stable multiple emulsions of droplets within droplets.[13,14] A recent study reviews the impact of channel geometry, cross- or co-flowing, on stable emulsion creation,[15] showing advantages of both methods.

Above a certain limit, droplet size is strongly dependent on the flow rate ratio.[16] Both cross- and co-flowing droplet forming devices are generally controlled by the ratio of the continuous to

[a]*Mechanical Engineering, University of Massachusetts, Amherst, MA, 01003, USA. E-mail: rothstein@ecs.umass.edu*
[b]*Mechanical Engineering, University of Texas, Dallas, TX, 75080, USA*

dispersed phase flow rates; the continuous phase flow rates often being an order of magnitude, or more, greater than the dispersed phase. In addition to flow ratio, other passive formation processes control total volume flow rate or pressure. More recent work using a novel single layer valve design has allowed drop size and frequency to be controlled by changing the flexible channel neck geometry with pneumatic pressure *in situ*;[17] this is considered an active formation process. Other active concepts include multi-layered devices with elastomeric switching valves,[18,19] thermal control through the local heating from a focused laser,[20] and electrostatic control by using electro-rheological (ER) fluids.[21] While these active processes present a good opportunity for direct feedback control, they rely, in most cases, on much more complicated devices, equipment, and even very elegant fluids doped with exotic particles. The strength of the passive formation processes, and the reason they are employed in a large portion of the microfluidic droplet research, is that they require basic laboratory tools (syringe pumps) and simple devices making them accessible to a spectrum of scientific explorations. In many of the aforementioned droplet formation methods, surfactants are often used to prevent the droplets from coalescing, thereby stabilizing the resultant emulsions.

The standard methods for fabricating microfluidic devices were inherited from the microelectronics industry.[22,23] Photoresists or etch resists are patterned onto a substrate, most commonly silicon, with photo- or electron-beam-lithography; micrometre size features with ever-increasing aspect ratios can be patterned cheaply and reliably with these methods. Using soft-lithography, these pattern masters, either positive or negative and in single or multiple layers, are transferred into soft polymers such as PDMS. These PDMS devices can be easily sealed and interconnected, and when adhered to a glass substrate by simple oxidation methods, such microchannels have become the research standard.[4,24] In the creation of droplets in microchannels, surface effects are particularly important. The widely used PDMS devices, with hydrophobic walls, are ideal for water-in-oil emulsions, but can prevent successful droplet formation in other situations. PDMS devices can be surface-modified with chemical treatments,[25] including a plasma/ozone exposure for easy but temporary success,[26] and more permanently by grafting hydrophilic polymers inside the microchannels.[27] Alternative surfaces are available with hard polymers, such as polycarbonate, which can be directly laser ablated to form simple microchannel geometries.[28] Additional fabrication methods borrowed from other industries include nano-imprint lithography and hot embossing in other hard polymers and glass.

Highly intricate microchannel arrays with valves, multiple layers, and careful inlet/outlet control have been used to successfully develop microfluidic devices for applications as complex as protein crystallization[8] and fluidic analogs of random access memory chips.[29] Both micro- and nanofluidics are finding increasing use in the growing toolbox of nanotechnology. Microfluidic devices are already being used as micro-reactors to produce nanoparticles *via* carefully controlled chemical reactions.[30] These laboratories on a chip hold vast potential for industrial application, however, only the most simple are truly starting to emerge as commercially viable, particularly in the area of droplet formation and emulsion creation (RainDance™ RainStorm, Fluigent MFCS-4C).

Even without overly complex design, requiring multiple layers and valving, simple microfluidic devices can currently produce droplets on the order of a few micrometres in diameter, with good repeatability.[11] Smaller droplets on the order of 20 nanometres have been created with the extreme shear present in colliding jet geometries, however, these are far more chaotic and offer very little control of size dispersity.[6] Further complicating controlled production, the issue of droplet coalescence becomes extremely difficult to control at these small sizes. Stabilization of droplets with surfactants results in a baseline limit of droplet size on the order of tens of nanometres due to the physical size of the micelles which are formed. Despite these difficulties, the stable and orderly production of droplets using co- and cross-flowing geometries exists as a possible solution, through optimization, for creation of nano-emulsions.

To date, the approach to optimizing the droplet formation process has focused on understanding the underlying physical behavior. This has most recently been done, in great detail, with respect to channel geometry as well as all relevant fluid properties.[31] In contrast, the approach described in this paper is based on using feedback control theory, thereby eliminating the need for prior knowledge of the working fluids. We present the design of a microfluidic-based technology utilizing relatively simple microchannel geometries in combination with a closed loop feedback system to control the continuous and dispersed phase flow rates in order to automate the production of an emulsion with a desired size and dispersity. Optimization of a controlled microdevice pumping system to allow for a tunable emulsion is in itself a novel project; however, the ultimate goal is for the entire system, device geometry and control, to be developed to a point that will allow the device to reach nanoscale emulsions in the future.

2. Experimental

Microchannel design and fabrication

The microfluidic devices which served as the basis for the present study were fabricated from poly(dimethylsiloxane) elastomer (PDMS, Dow Sylgard 184) using standard soft-lithography fabrication techniques.[23] Device masters were patterned on silicone wafers *via* photolithography using epoxy based negative photoresist (MicroChem SU-8), and molded in PDMS. Standard glass microscope slides were spin-coated with a thin layer of PDMS and the molded devices were then bonded to the slides using a simple PDMS-ratio mismatch to provide uniform surface properties within the channels. More details of the specific fabrication procedure can be found in previous work.[24,32]

A basic flow-focusing geometry was selected for use in this study, the dimensions of which are shown in Fig. 1. The inner channel, with a contraction width of $w_c = 25$ μm, delivers the droplet forming dispersed phase at a flow rate denoted Q_d. Two outer channels, having a width of $w_u = 200$ μm, converge at an angle of 60° to horizontal and provide the co-flowing outer, or continuous phase at a flow rate denoted Q_c. The downstream channel width is $w_d = 400$ μm and the device is molded with a uniform channel depth of $h = 150$ μm to minimize the degree to which large droplets are squeezed between the top and bottom of the channel. The relatively large geometry was selected primarily

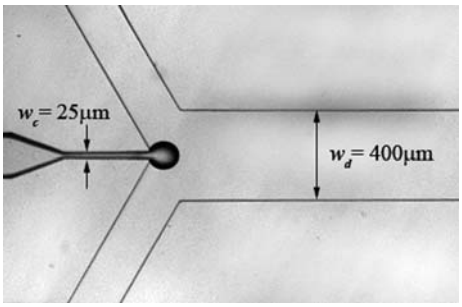

Fig. 1 Flow-focusing geometry used for all experiments. The microchannel dimensions include a focusing contraction width, $w_c = 25$ μm, downstream channel width, $w_d = 400$ μm, and uniform channel depth, $h = 150$ μm.

for this proof-of-concept study to allow the widest possible range of droplet sizes.

Pumping and control apparatus

Flow through the microchannels is driven by two stepper-motor actuated micro-syringe pumps (New Era Pump Systems, NE-500 OEM) *via* glass syringes: a 500 μl syringe (Hamilton, Microliter™ #750) for the dispersed phase and a 1 mL syringe (Popper & Sons, Perfektum®) for the continuous phase. Although the syringe pumps incorporate a high precision micro-stepped motor driver, syringe sizes were kept as small as practically possible to reduce the possibility of observing flow rate fluctuations. The system is connected with polyethylene tubing (BD Intramedic) fitted over 22 g blunt tip dispensing needles (Brico Medical, BN2205). The pumps, which are assigned a semi-permanent address number so they can be addressed individually, are connected in serial with RJ-11 terminated network cables to the COM port of a desktop computer and communicate *via* RS-232. All pump commands and status queries are sent and handled, respectively, by a virtual instrument (VI) developed in the LabVIEW graphical programming platform (National Instruments™).

Experiments are performed on an inverted microscope (Nikon TE2000) using a 4× lens and images are captured using a high-speed CCD camera (Vision Research, Phantom v4.6). The camera is connected *via* Ethernet to the same computer and VI as the pumps. Droplet detection is performed within the VI using a routine developed with the aid of tools in the Vision Development Module for LabVIEW. The routine performs a binary threshold based on the droplet intensity, fills enclosed spaces, and uses a circle filter to remove objects that do not fall within a narrow range of circularity. This circularity parameter is simply a ratio of the largest diameter to the area and is used to not only remove the rectangular channel objects, but also to prevent the routine from analyzing large slugs of fluid from a poorly operating flow-focusing process or even coalesced droplets. The remaining circles, or droplets in the resulting binary image, are analyzed and the number of droplets as well as their average diameter is output for each image. It should be noted that image acquisition was performed on a straight section of channel, identical in size and field of view to Fig. 1, but several channel widths downstream from the flow-focusing tip so that only fully formed and freely flowing droplets were analyzed.

The VI itself functions primarily within a continuous while loop. In each iteration of the loop, an image is pulled from the camera and processed while the pumps are simultaneously queried for their current pumping status. In open-loop mode, the outputs of each loop are the resulting droplet diameter, which is recorded in a text file, and a new serial command, which is compiled based on the manually entered flow rate to be sent back to the pumps. In closed-loop mode, the automatic control loop within the VI is closed by feeding back the measured droplet diameter, d, into a PI controller which outputs the necessary resultant flow rate ratio, $\bar{Q}_r = Q_c/Q_d$, based on a manually entered desired droplet diameter. A conditional statement then sends an updated flow rate to the pumps.

Test fluids

The continuous phase liquid in all experiments was a household grape seed oil with a viscosity of $\mu = 81$ cP and was pumped at a maximum flow rate of $Q_c \leq 100$ μl min^{-1}. For the simplest immiscible combination, all dispersed phase liquids were aqueous, using Millipore filtered water, and in all experiments reported in this study, the dispersed phase was pumped at uniform flow rate of $Q_d = 2$ μl min^{-1}. In order to test and fine-tune the controller, non-Newtonian solutions were also tested. A polymer solution was made using a poly(ethylene glycol) with a molecular weight, $M_w = 2.7 \times 10^6$, and a critical overlap concentration, $c^* > 0.10$ wt%.[33] A concentration of [PEG] = 0.05 wt% was used to remain well within the dilute regime while still imparting some viscoelastic properties. Another weakly viscoelastic solution was made using the cationic surfactant cetylpyridinium chloride (CPyCl). With a critical micellar concentration of $CMC_{CPy,H_2O} = 0.9$ mM,[34] solutions were prepared at and above this critical point: 0.9 mM (0.031 wt%), 2 mM (0.068 wt%), and 5 mM (0.170 wt%). This range of solutions provided a test for not only weakly viscoelastic effects of micelles, but also the effect of lowering interfacial tension between the oil and aqueous phases; continuous and dispersed, respectively.

A complete rheological dataset for each of the commonly used test fluids in this study can be found in the literature[24,32–37] and will not be duplicated here for the sake of brevity. However, it is important to note that quantifying the elastic properties of such dilute viscoelastic solutions is difficult even with the most sensitive shear rheometers.[33] Previous work with similar PEG solutions has reported both shear-thinning and frequency dependent dynamic moduli.[36] Extensional rheometry can be used to measure the extensional viscosity and calculate a Trouton ratio as the ratio of the transient extensional viscosity to the zero shear-rate viscosity, $Tr = \eta_E/\eta_0$. For a Newtonian fluid, the Trouton ratio is a constant value of $Tr = 3$, but for elastic fluids it can be much higher.[35] The presence of a large extensional viscosity can stabilize a fluid jet, slow its breakup into drops and affect the size and periodicity of drops formed within a flow focusing device.[38] Several previous works using different types of extensional rheometers have shown that both highly dilute PEG and CPyCl solutions have $Tr > 3$, in some cases orders of magnitude higher.[35,37,39] Furthermore, it has been shown directly

in phenomenological microfluidic studies that despite possessing elasticity so weak that it hardly registers in bulk rheometric measurements, dilute solutions of PEG and CPyCl exhibit dramatically different behavior than their Newtonian analogs.[32,36]

3. Results and discussion

Open-loop droplet production model

In the flow-focusing junction, one of the most simple and effective droplet forming geometries, droplets of the dispersed phase are formed by a combination of shear and extensional flow. The strength of the outer continuous phase shears the interface of the dispersed phase, while the dispersed phase itself is undergoing an extension-dominated flow as it emerges from the narrow focusing tip. At relatively low flow rates, the emerging dispersed phase interface nearly blocks the downstream flow of the continuous phase liquid. A large upstream pressure is formed which eventually squeezes the neck of the dispersed phase and causes the droplet to pinch off.[31] Although interfacial tension plays a part at this stage, driving droplet formation on its own, even in a relatively weak flow, it is the strength of the continuous phase flow rate, or rather the flow rate ratio, that has the greatest effect on droplet size. Additionally, while interfacial tension and geometry factors all play a role in droplet size, only flow rate can be controlled in real-time within a single experimental device without the use of elastomeric valves or special fluids.

Before making a final choice for the controlling flow parameter, several experiments were performed in order to investigate the effects of varying both flow rate ratio and total volume flow rate. Steady flow curves were generated by first varying the flow rate ratio, $\bar{Q}_r$, for three different fixed dispersed phase flow rates, $Q_d = 1$, 2, and 3 μl min^{-1} and then by varying the total flow rate while keeping the flow rate ratio fixed at $\bar{Q}_r = 5$. The resultant droplet size data are shown in Fig. 2 for a dispersed phase of water and a continuous oil phase. In Fig. 2, the droplet size is normalized by the downstream channel width, $\bar{d} = d/w_d$. In the experiments at a fixed dispersed phase flow rate, the droplet size was found to decrease quickly as a function of increasing flow rate ratio. Increasing the fixed dispersed phase flow rate slightly increased the speed of response curve, such that the droplet size was smaller for all $\bar{Q}_r$. Although a faster response is desirable, it comes at the cost of an increased total volume of flow and therefore pressure within the device. In the experiments performed at a constant flow rate ratio, the droplet size was found to decrease with total flow rate as well. Each dataset in Fig. 2 was carried out to nearly the same total flow rate, and therefore, if one compares the final points in all cases, it becomes clear that varying flow rate ratio resulted in a greater change in droplet size than varying continuous phase flow rate. Based on these results, flow rate ratio was selected as the controlled variable in order to best accomplish the goals of this study. For the purpose of uniformity and simplicity in reporting, the dispersed phase flow rate was fixed at $Q_d = 2$ μl min^{-1} for all remaining experiments presented in this study.

As discussed in Section 2, the devices used in this study have a rectangular cross-section, where the height, $h = 150$ μm, is less than the downstream channel width, $w_d = 400$ μm. In practice, this means that any circular droplet with a measured diameter greater than the channel height is in fact disc-shaped as a result of being compressed between the top and bottom walls of the microchannel. It should be reiterated that the image processing routine employed in our VI does not allow for compression of droplets between the side walls, $d > w_d$. Due to the use of a circularity filter, such shapes would be eliminated as large slugs and not measured. To calculate the volume, V, or the unconstrained diameter, d_{corr}, of the drops, a corrective algorithm can be employed based on the assumption that the total volume of a circular compressed disc is equal to the sum of a cylinder with

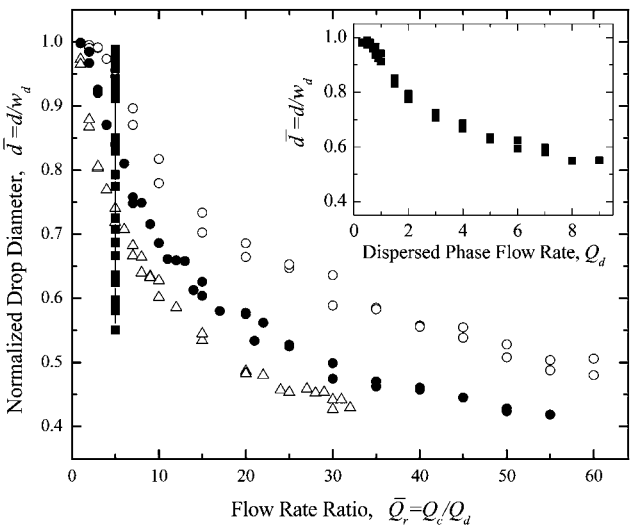

Fig. 2 Open-loop flow curves for droplet diameter, normalized by downstream channel width, as a function of both flow rate ratio and total volume flow rate (inset). The data include fixed $Q_d = 1$ (open circles), 2 (closed circles), and 3 (open triangles) μl min^{-1}, as well as fixed $\bar{Q}_r = 5$ (closed squares). Pure water is the dispersed phase in all cases.

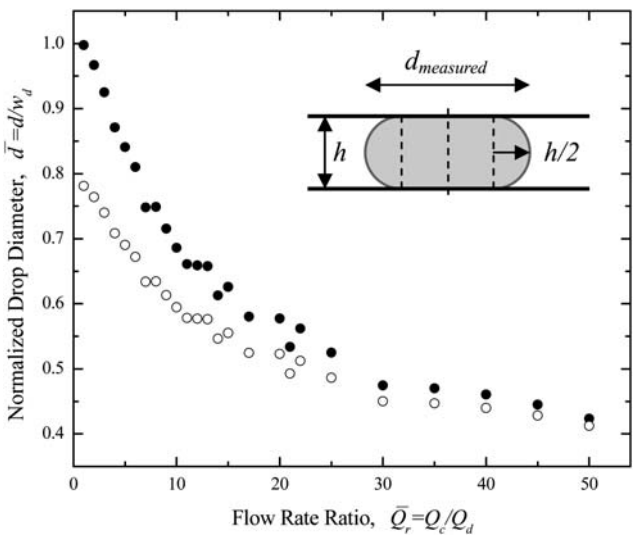

Fig. 3 Open-loop flow curves for normalized droplet diameter both as measured (closed circles) and geometrically corrected (open circles) to account for being constrained by the microchannel into a disc-like shape. Inset figure shows a schematic of a disc-like droplet in profile.

a diameter $d - h$ plus a revolved semicircle with diameter h (a schematic is included in Fig. 3):

$$V = \left[\frac{\pi}{4}(d-h)^2 h\right] + \left[\frac{\pi^2 h^2}{4}\left(\frac{d-h}{2} + \frac{2}{3\pi}h\right)\right] \quad (1)$$

If a given droplet with a volume calculated using eqn (1) is allowed to move into an open channel and assume a spherical shape, its diameter can be calculated as:

$$d_{corr} = 2\left(V\frac{3}{4\pi}\right)^{1/3} \quad (2)$$

Eqn (1) and (2) can now be used to produce a corrected droplet size flow curve, which is shown in Fig. 3 for the representative data of water at $Q_d = 2$ μl min^{-1}. As expected, there is a large correction of nearly 20% at large measured diameters, which vanishes as the measured diameter approaches the channel height at $\bar{d} = 0.375$. Such a correction algorithm is fairly simple to implement and becomes important when either volume or spherical droplet size is critical, such as in the application of emulsion creation. However, if the application is simple and is fully constrained to a single device within a uniform and constant depth channel, the effective spherical measurement of a droplet is less important than the measured diameter. The latter applies to this microfluidic device, and therefore, the correction has not been applied. For the remainder of the data presented, droplet size is reported based on the measured diameter as imaged, rather than corrected diameter.

The first step in designing the control system was to understand the plant; in this system, the plant is simply the flow-focusing device itself, where the input is the controlled variable, flow rate ratio, and a uniform droplet size is the output. Steady flow curves and temporal step response data were collected for several fluid phases. Normalized droplet size, $\bar{d}$, as a function of flow rate ratio, $\bar{Q}_r$, is shown in Fig. 4 for all test fluids discussed in Section 2. The data for all liquids show droplet size decreasing in a roughly exponential decay with increasing flow rate ratio. Addition of the dilute polymer, PEG, as well as surfactant below the CMC (the data for [CPyCl] = 0.9 mM are not included in Fig. 4) resulted in essentially no change from pure water. However, the higher concentration surfactants, 2 mM and 5 mM, did yield smaller drop sizes, nearly an order of magnitude of drop size variation was attained, by transitioning from a squeezing regime to a jetting regime. Droplet forming regimes and the effect of surfactants have been reviewed in detail by previous work,[31] and will be discussed further in a following section as they relate to the goal of control.

In order to approximate a plant model for the system, temporal step response data were fit with a first order model. The response of water droplet size to step changes in flow rate ratio over time is shown in Fig. 5. Analysis of this data yielded an average process gain, $K_p = -14.38$, and reset time, or open-loop time constant, $T_{p,open} = 7.75$ s. From these parameters, a simple first-order plus dead time (FOPDT) dynamic transfer function model[40] for the plant could then be defined directly in Laplace-space:

$$G(s) = \frac{K_p}{T_p s + 1} = \frac{-14.38}{7.75s + 1} \quad (3)$$

Using this transfer function, a simulated response to the same flow ratio step input was generated and is superimposed on the collected droplet size data in Fig. 5. While the simple first-order model cannot capture the real system exactly, especially for larger step inputs where the droplet size response becomes smaller (as evidenced by the shape of the data in Fig. 4), comparison of the real and simulated data shows good agreement at low and moderate flow rate ratios. A noteworthy feature of the data is the disappearance of droplets in response to a larger positive step in $\bar{Q}_r$, as for $t = 100$ s in Fig. 5. This is a real observation and is explained by the large and fast change in

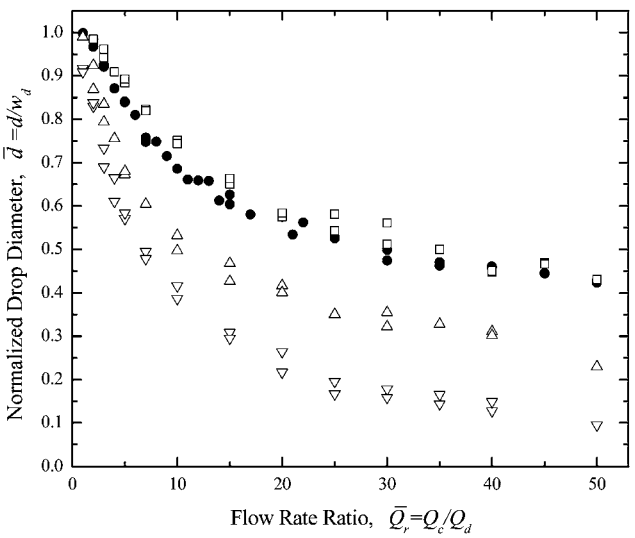

Fig. 4 Open-loop flow curves for normalized droplet diameter as a function of flow rate ratio, and for varying dispersed phases including water (closed circles), 0.050 wt% PEG (open squares), 0.068 wt% CPyCl (open up triangles) and 0.170 wt% CPyCl (open down triangles). All data are for a dispersed phase flow rate of $Q_d = 2$ μl min^{-1}. Data were recorded both for increasing and decreasing flow rate ratio to check for hysteresis.

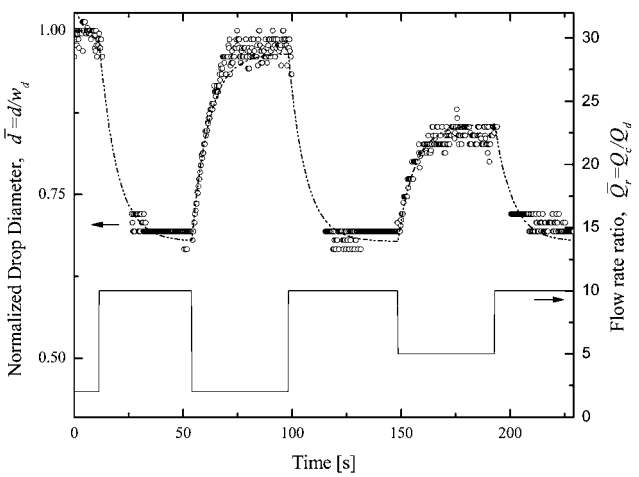

Fig. 5 Open-loop device response for water as the dispersed phase, in terms of droplet diameter (open circles), to step inputs in flow rate ratio (solid line). The simulated response of a simple first-order transfer function model with $K_p = -14.38$ and $T_p = 7.75$ is superimposed over the diameter data (dashed line).

upstream pressure which essentially blocks the dispersed phase from emerging downstream. As equilibrium is reached, the dispersed phase meets the now stronger continuous phase flow and emerges almost immediately at the new smaller droplet size. The overall time constants for positive and negative step inputs ultimately are the same. However, this lack of data over a short period of time presents issues for control implementation, and will be addressed in the following section.

Closed-loop feedback control

Having a reasonably accurate first-order plant model, a standard and basic PID control approach was added to the virtual instrument, with a negative feedback loop for droplet diameter. A simplified block-diagram schematic of the droplet production device is shown in Fig. 6. After initial experimentation and tuning, it was found that the extra damping provided by the derivative term was not necessary, and PI control was sufficient. The FOPDT dynamic model guidelines were used to calculate the initial gains for the PI control. These values are based on the open-loop process gain and open-loop time constant and allow for the calculation of aggressive, moderate, or conservative controller gains.[40] Use of the open-loop parameters shown in eqn (3) resulted in a first guess for proportional gain of $K_c = 0.067$ and an integral, or reset-time, of $T_i = 7.75$ s, equal to that of the open-loop time constant. This conservative algorithm yields a closed-loop time constant that is one order of magnitude greater than the open-loop time constant, $T_{p,closed} = 77.5$ s. Further fine tuning, both manual and automatic, using National Instruments Control Design and Simulation tools, yielded the following PI controller transfer function:

$$D(s) = K_c\left(1 + \frac{1}{T_i s}\right) = -0.08\left(1 + \frac{1}{17.9s}\right) \quad (4)$$

As mentioned in the previous section, large positive step inputs resulted in a lack of data for a period of a few seconds as the continuous and dispersed phase flow rates reach equilibrium before droplets can emerge past the upstream pressure. In tuning the PI controller, this feature caused aggressive and even moderate gain values to result in an unstable system, either with oscillations or, more typically, saturation of the controller output. To address this issue in practice, a hard limit was imposed on the output (in terms of flow rate) to protect the pumps and devices, and an anti-windup scheme was included in the PI function. With these additions in place, the final PI controller in eqn (4) had a longer integral time than the initial FOPDT estimate, $T_i = 17.9$ s, necessary to slow down the controller output ramp for large positive steps, but could support a slightly larger proportional gain, $K_c = 0.080$. Sample time was limited by the speed of the image analysis routine on the available

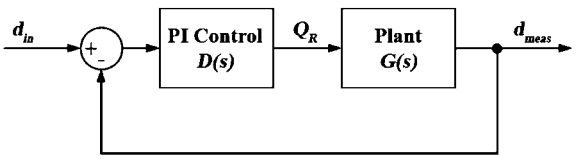

Fig. 6 Block diagram for the droplet production process with negative feedback loop for control of droplet diameter.

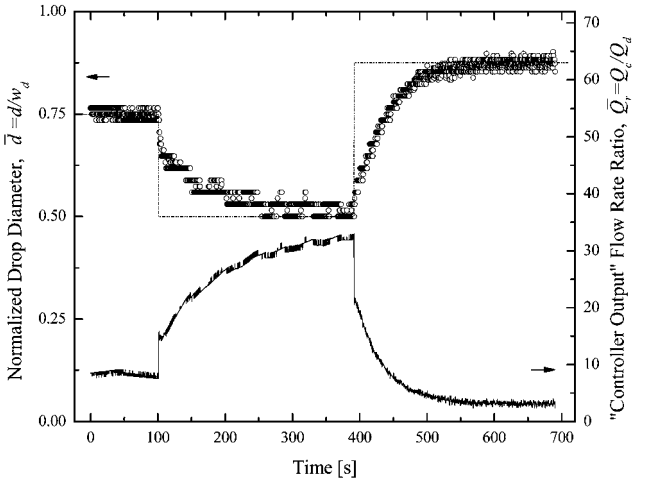

Fig. 7 Closed-loop device response using PI control for water as the dispersed phase. The data include: controller output in terms of the required flow rate ratio (solid line), the controlled device, or plant, response in terms of droplet diameter (open circles), as well as the diameter set point (dashed line).

desktop computer, to $f_s = 4$ Hz. In comparison to the speed of the physical fluid response, on the order of tens of seconds, however, this sample rate was sufficiently fast.

A typical closed-loop device response is shown in Fig. 7, with pure water as the dispersed phase. These data demonstrate successful automatic control for step inputs that cover the majority of the achievable diameter range for the water and oil phase combination, $0.50 \geq \bar{d} \geq 1.0$ (reference Fig. 4). Although the observed closed-loop time constant is rather large, $T_p > 100$ s, the controller output is stable and the steady-state error in diameter is minimized. There is a degree of noise in the closed-loop response, on the order of ±5% (±20 μm). For the purpose of comparison, an open-loop response was manually constructed to result at similar values of diameter, as shown in Fig. 8. While the

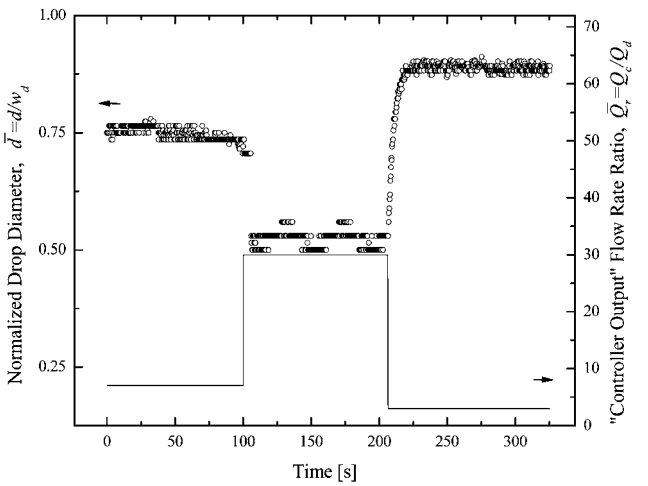

Fig. 8 Open-loop device response for pure water as the dispersed phase, in terms of droplet diameter (open circles), to step inputs in flow rate ratio (solid line). The droplet diameters in these data are set to match those of Fig. 7 in order to compare relative noise in the signal.

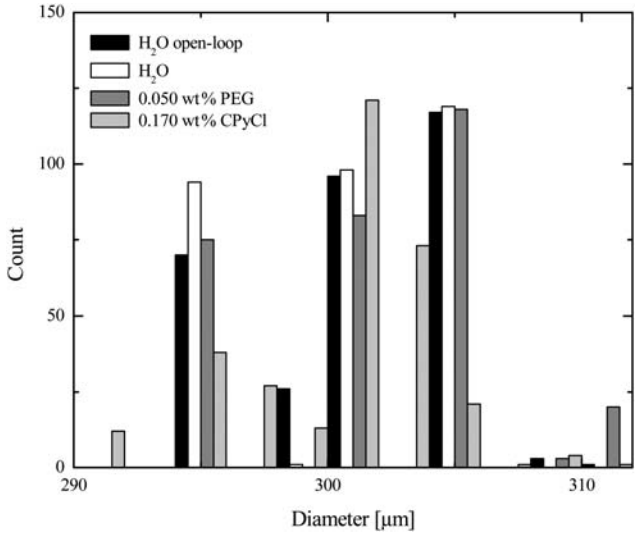

Fig. 9 Diameter data shown as a histogram confirming that open and closed loop response have nearly identical distribution in data, due to experimental/image-processing factors alone.

discrepancy in open and closed loop time constants is obvious, it can be observed that the level of general measurement noise in the diameter data is consistent in both cases. Therefore, it can be stated that the closed-loop controller does not amplify the noise in the signal, and although it is slow, at the current stage, it produces a highly stable response.

A quantitative analysis of the noise in the diameter measurement was performed by plotting a histogram of 300 data points recorded at steady-state for all fluid phase combinations, and for both the open- and closed-loop experiments for pure water. In Fig. 9, we observe that all experimental cases, including the non-Newtonian phases to be discussed in the following section, show a nearly identical histogram distribution. It should be noted that each diameter data point or sample is the result of a single image. The image analysis routine measures all droplets in a given image and outputs an average diameter. Therefore, due to droplet spacing, at low flow rates each sample is the result of an average of several drops in the single image, while at higher flow rates, often only a single droplet is present in the interrogation region of the channel. This averaging is part of the data-acquisition for both open and closed-loop responses.

Control of non-Newtonian liquid phases

One of the primary benefits resulting from the implementation of automatic feedback control in a droplet production device is the ability to quickly produce droplets of a desired size with any two immiscible phases. Knowledge of properties such as interfacial tension and viscosity is unnecessary as long as the desired drop size is reasonable given the dimensions of the flow-focusing geometry. To demonstrate the efficiency of the PI controller, two non-Newtonian solutions were tested. The results are shown in Fig. 10, using the same set point profile as with the experiments using water as the dispersed phase, shown in Fig. 7.

The results for the PEG solution in Fig. 10(a) are nearly identical to those for water (Fig. 7), with similar overall dynamics

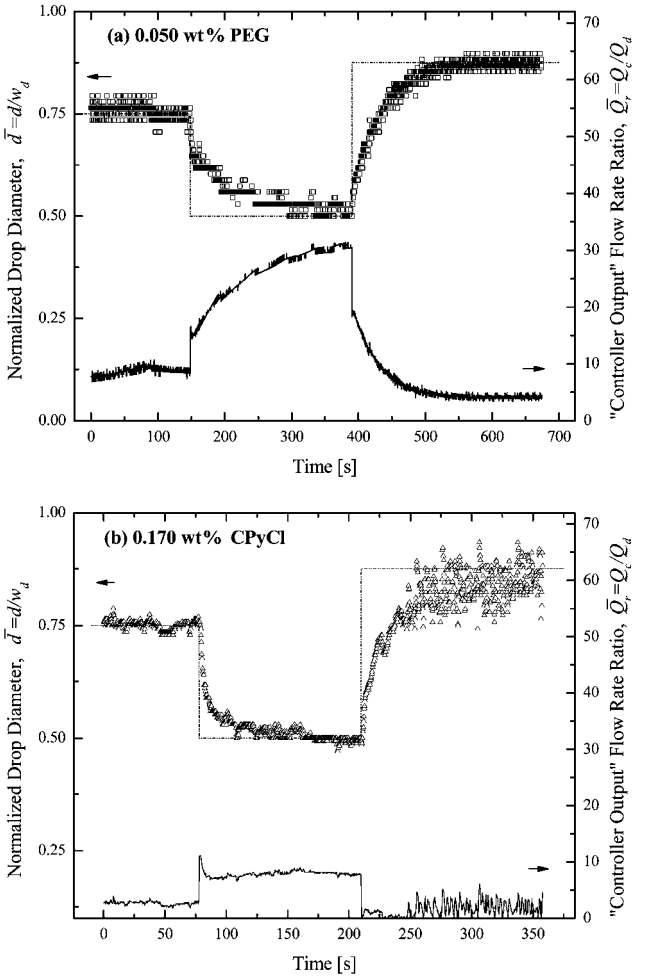

Fig. 10 Closed-loop device response for (a) 0.050 wt% PEG and (b) 0.170 wt% (5 mM) CPyCl as the dispersed phase. The commanded set point profile and plot axes match Fig. 7, for comparative purposes. The spread in the data of (b) at large times demonstrates the stability of the controller even when the set point is outside the range of droplet diameters that can be obtained within the device for the given fluid.

and amount of noise in both diameter and controller output. In the initial step from $\bar{d} = 0.75$ to $\bar{d} = 0.50$, there is a short period with no droplets produced due to the increased pressure drop, for reasons discussed previously. The controller does not saturate and compensates to a lower value once droplets re-emerge. Droplets of PEG were observed to be regular in form, and little difference from water could be distinguished; this could be expected from the similar flow curves observed for both phases, shown in Fig. 4. Previous drop formation experiments with higher molecular weight polymer solutions, $M_w \geq 2 \times 10^6$, did not exhibit any secondary droplet formation due to the higher relative magnitudes of elastic stress and capillary pressure.[33] Although this is dependent both on concentration and molecular weight, keeping consistently below the overlap concentration supported this observation.

In a final set of experiments, the 5 mM CPyCl surfactant solution was used. Unlike the experiments using water or PEG as the dispersed phase, the data for CPyCl droplets do not exhibit the pressure blockage with a step to smaller droplet size; droplets

were produced almost continuously, as shown for $t = 75$ s in Fig. 10(b). Another more striking observation is the very large amount of spread in that data for $t > 200$ s, where the set point was changed to $\bar{d} = 0.875$. This can be explained by the fact that the droplet diameter profile for the CPyCl solution is quite different, as shown in Fig. 4 where the flow curve does not quite reach $\bar{d} = 1$ even for a flow ratio of $\bar{Q}_r = 1$, which was the lowest possible value. Despite the physical inability to obtain the set droplet diameter, the controller does not oscillate out of control; an interesting side-result and demonstration of the controller stability. A final observation is the speed of the response. In the step from $\bar{d} = 0.75$ to $\bar{d} = 0.50$, the response in Fig. 10(b) reaches steady-state in approximately 125 s, nearly half the time required for the PEG or water. The reason for this is more apparent in terms of the controller output. Where both PEG and water require a flow rate ratio of approximately $\bar{Q}_r = 30$ to achieve a diameter of $\bar{d} = 0.50$, the CPyCl phase requires a ratio of only $\bar{Q}_r \simeq 9$ for the same droplet size. This is once again supported by the flow curves shown in Fig. 4. The smaller controller output necessary to achieve the step in drop size explains the increased speed of the response in the case of the surfactant phase. Collectively, these quantitative observations lead directly to another feature highlighted by the surfactant experiments: the closed-loop controller was able to successfully control droplet size in multiple droplet producing regimes.

As mentioned previously, the addition of surfactant to the aqueous dispersed phase in the flow-focusing experiments resulted in a flow regime transition. The series of images in Fig. 11 are representative of the most basic squeezing regime, and were typical of those observed for both pure water and the PEG solution. However, with the addition of surfactant, the flow undergoes a transition from squeezing to jetting with surfactant mediated thread formation. In this flow regime, surfactant moves to the interface and is swept into a thin, surfactant-rich thread with very low interfacial tension; details of this mechanism have been described previously in great detail.[31] A stable jet of the dispersed phase extends far from the flow-focusing tip and can produce droplets smaller than that of the critical width, w_c. Although this can occur without surfactant, the addition of surfactant and the subsequent threads also results in the formation of very small secondary satellite droplets that result from the thread breaking up due to very large strains. This behavior is shown in Fig. 12 and for the 5 mM CPyCl solution used, the transition occurs at approximately $\bar{Q}_r = 20$. It should be noted that the current device does not track and measure satellite droplets. They are below a size threshold for the image processing which focuses only on the primary drop. Future work is planned to add this functionality and investigate both primary and satellite droplet formation and control.

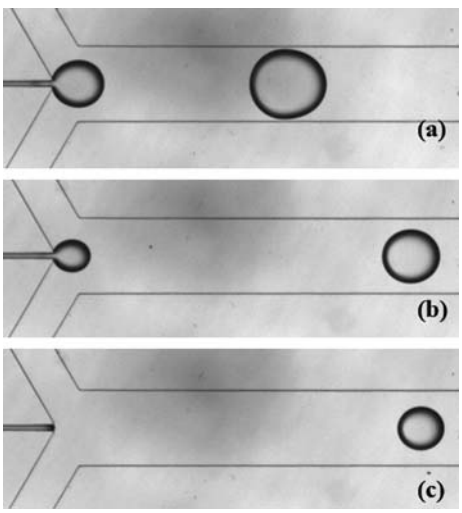

Fig. 11 Photographs of droplet production with water as the dispersed phase. Images are for three flow rate ratios: (a) $\bar{Q}_r = 2$, (b) $\bar{Q}_r = 10$, and (c) $\bar{Q}_r = 20$.

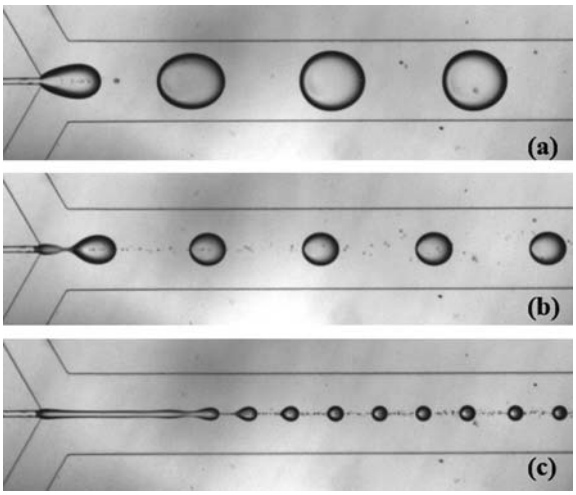

Fig. 12 Photographs of droplet production with 5 mM (0.170 wt%) CPyCl as the dispersed phase. Images are for three flow rate ratios: (a) $\bar{Q}_r = 2$, (b) $\bar{Q}_r = 10$, and (c) $\bar{Q}_r = 28$.

4. Conclusions

This study has successfully demonstrated proof-of-concept in the implementation of an automatic closed-loop PI control system with negative feedback in the production of droplets in a microfluidic device. A standard flow-focusing microchannel geometry was used to generate droplets over nearly an order of magnitude in size, ranging from $d = 400$ μm to $d \simeq 40$ μm. The immiscible liquids used were household oil as the continuous phase and aqueous dispersed phases. A PI controller was implemented within a virtual instrument developed to process and measure droplet images while controlling the flow rate ratio *via* two computer-controlled syringe pumps. Tuned with a conservative proportional gain and integral time, the control system was able to successfully produce the required droplet size with minimal noise and no systematic steady state error. Additionally, the device and controller were able to produce desired droplet size with both pure water and non-Newtonian dispersed phases, including a PEG polymer solution and CPyCl surfactant solutions. Future work is planned to address the conservatively long closed-loop time constant necessary to accommodate the stoppage of droplet production caused by upstream pressure

increases. In order to design highly monodisperse emulsions, with change possible in real-time, this must be addressed and a faster response achieved.

The production of droplets in microfluidic devices has been developed and utilized for a number of applications, including micro-chemistry and emulsion production. Implementing automatic control over droplet size and the ability to process any combination of immiscible fluids without detailed prior study of their interfacial properties opens the door to even more possibilities. It is envisioned that through further tuning of both the flow-focusing geometry as well as the control scheme, even smaller droplet size scales can be attained, allowing the production of custom micro- and nano-emulsions with tailored size and dispersity.

Acknowledgements

The authors would like to thank the National Science Foundation for support of this research through the Center for Hierarchical Manufacturing at the University of Massachusetts.

References

1 G. M. Whitesides, *Nature*, 2006, **442**(7101), 368–373.
2 A. Manz, D. J. Harrison, E. M. J. Verpoorte, J. C. Fettinger, A. Paulus, H. Ludi and H. M. Widmer, *J. Chromatogr.*, 1992, **593**(1–2), 253–258.
3 T. M. Squires and S. R. Quake, *Rev. Mod. Phys.*, 2005, **77**(3), 977–1026.
4 S. L. Anna, N. Bontoux and H. A. Stone, *Appl. Phys. Lett.*, 2003, **82**(3), 364–366.
5 G. F. Christopher and S. L. Anna, *J. Phys. D: Appl. Phys.*, 2007, **40**(19), R319–R336.
6 K. Meleson, S. Graves and T. G. Mason, *Soft Matter*, 2004, **2**(2–3), 109–123.
7 J. Husny and J. J. Cooper-White, *J. Non-Newtonian Fluid Mech.*, 2006, **137**(1–3), 121–136.
8 D. R. Link, S. L. Anna, D. A. Weitz and H. A. Stone, *Phys. Rev. Lett.*, 2004, **92**(5), 054503.
9 T. Nisisako, T. Torii and T. Higuchi, *Lab Chip*, 2002, **2**(1), 24–26.
10 Q. Y. Xu and M. Nakajima, *Appl. Phys. Lett.*, 2004, **85**(17), 3726–3728.
11 S. L. Anna and H. C. Mayer, *Phys. Fluids*, 2006, **18**(12), 121512.
12 A. M. Ganan-Calvo and J. M. Gordillo, *Phys. Rev. Lett.*, 2001, **87**(27), 274501.
13 A. R. Abate and D. A. Weitz, *Small*, 2009, **5**(18), 2030–2032.
14 L. Y. Chu, A. S. Utada, R. K. Shah, J. W. Kim and D. A. Weitz, *Angew. Chem., Int. Ed.*, 2007, **46**(47), 8970–8974.
15 A. R. Abate, A. Poitzsch, Y. Hwang, J. Lee, J. Czerwinska and D. A. Weitz, *Phys. Rev. E: Stat. Phys., Plasmas, Fluids, Relat. Interdiscip. Top.*, 2009, **80**(2), 026310.
16 Y. P. Hong and F. J. Wang, *Microfluid. Nanofluid.*, 2007, **3**(3), 341–346.
17 A. R. Abate, M. B. Romanowsky, J. J. Agresti and D. A. Weitz, *Appl. Phys. Lett.*, 2009, **94**(2), 023503.
18 T. Thorsen, R. W. Roberts, F. H. Arnold and S. R. Quake, *Phys. Rev. Lett.*, 2001, **86**(18), 4163–4166.
19 M. A. Unger, H. P. Chou, T. Thorsen, A. Scherer and S. R. Quake, *Science*, 2000, **288**(5463), 113–116.
20 C. N. Baroud, M. R. de Saint Vincent and J. P. Delville, *Lab Chip*, 2007, **7**(8), 1029–1033.
21 X. Z. Niu, M. Y. Zhang, J. B. Wu, W. J. Wen and P. Sheng, *Soft Matter*, 2009, **5**(3), 576–581.
22 S. Brittain, K. Paul, X. M. Zhao and G. Whitesides, *Phys. World*, 1998, **11**(5), 31–36.
23 G. M. Whitesides and A. D. Stroock, *Phys. Today*, 2001, **54**(6), 42–48.
24 L. E. Rodd, T. P. Scott, D. V. Boger, J. J. Cooper-White and G. H. McKinley, *J. Non-Newtonian Fluid Mech.*, 2005, **129**(1), 1–22.
25 D. Bodas and C. Khan-Malek, *Microelectron. Eng.*, 2006, **83**(4–9), 1277–1279.
26 Y. Berdichevsky, J. Khandurina, A. Guttman and Y. H. Lo, *Sens. Actuators, B*, 2004, **97**(2–3), 402–408.
27 L. M. Fidalgo, C. Abell and W. T. S. Huck, *Lab Chip*, 2007, **7**(8), 984–986.
28 J. Husny, H. Y. Jin, E. C. Harvey and J. Cooper-White, *Smart Mater. Struct.*, 2006, **15**(1), S117–S123.
29 T. Thorsen, S. J. Maerkl and S. R. Quake, *Science*, 2002, **298**(5593), 580–584.
30 Y. J. Song, J. Hormes and C. S. S. R. Kumar, *Small*, 2008, **4**(6), 698–711.
31 W. Lee, L. M. Walker and S. L. Anna, *Phys. Fluids*, 2009, **21**(3), 032103.
32 L. E. Rodd, J. J. Cooper-White, D. V. Boger and G. H. McKinley, *J. Non-Newtonian Fluid Mech.*, 2007, **143**(2–3), 170–191.
33 V. Tirtaatmadja, G. H. McKinley and J. J. Cooper-White, *Phys. Fluids*, 2006, **18**(4), 043101.
34 J. Y. Lee, G. G. Fuller, N. E. Hudson and X. F. Yuan, *J. Rheol.*, 2005, **49**(2), 537–550.
35 J. J. Cooper-White, J. E. Fagan, V. Tirtaatmadja, D. R. Lester and D. V. Boger, *J. Non-Newtonian Fluid Mech.*, 2002, **106**(1), 29–59.
36 E. Miller and J. Cooper-White, *J. Non-Newtonian Fluid Mech.*, 2009, **160**(1), 22–30.
37 L. E. Rodd, T. P. Scott, J. J. Cooper-White and G. H. McKinley, *Appl. Rheol.*, 2005, **15**(1), 12–27.
38 K. V. Edmond, A. B. Schofield, M. Marquez, J. P. Rothstein and A. D. Dinsmore, *Langmuir*, 2006, **22**(21), 9052–9056.
39 J. P. Rothstein, *J. Rheol.*, 2003, **47**(5), 1227–1247.
40 D. J. Cooper, *Practical Process Control: Proven Methods and Best Practices for Automatic PID Control*, Controlguru.com (e-textbook), 2006.